

Road boundary estimation to improve vehicle detection and tracking in UAV video

ZHANG Li-ye(张立业)^{1,2}, PENG Zhong-ren(彭仲仁)¹, LI Li(李立)¹, WANG Hua(王华)³

1. School of Transportation Engineering, Tongji University, Shanghai 201804, China;
2. School of Traffic and Transportation Engineering, Changsha University of Science and Technology, Changsha 410076, China;
3. School of Economics and Management, Tongji University, Shanghai 200096, China

© Central South University Press and Springer-Verlag Berlin Heidelberg 2014

Abstract: Video processing is one challenge in collecting vehicle trajectories from unmanned aerial vehicle (UAV) and road boundary estimation is one way to improve the video processing algorithms. However, current methods do not work well for low volume road, which is not well-marked and with noises such as vehicle tracks. A fusion-based method termed Dempster-Shafer-based road detection (DSRD) is proposed to address this issue. This method detects road boundary by combining multiple information sources using Dempster-Shafer theory (DST). In order to test the performance of the proposed method, two field experiments were conducted, one of which was on a highway partially covered by snow and another was on a dense traffic highway. The results show that DSRD is robust and accurate, whose detection rates are 100% and 99.8% compared with manual detection results. Then, DSRD is adopted to improve UAV video processing algorithm, and the vehicle detection and tracking rate are improved by 2.7% and 5.5%, respectively. Also, the computation time has decreased by 5% and 8.3% for two experiments, respectively.

Key words: road boundary detection; vehicle detection and tracking; airborne video; unmanned aerial vehicle; Dempster-Shafer theory

1 Introduction

It is widely believed that the smooth operations of the intelligent transportation system (ITS) rely heavily on the traffic information. At present, different sensors have been developed for this purpose, such as microwave detectors, GPS and traffic cameras. Among those detectors, traffic cameras mounted on airborne platform (e.g., helicopters and unmanned aerial vehicle) have been considered to be a promising traffic information detection method. Compared with video cameras mounted on traffic lights, bridges or poles, airborne camera could cover large road extent and is flexible to employ, which can capture high-resolution spatial-temporal traffic information, such as vehicle trajectory, lane changes and direct measure of density.

Helicopter with camera plays an important role in traffic flow theory study, which even dates back to 1927 [1]. Beginning in the late 1990s, many import ideas on the use of airborne imagery for traffic study were investigated and tested in the field [2–3]. UAV is another alternative airborne platform for traffic information

collection, which shows a promising platform with the development of UAV technologies. Compared with manned helicopter, it has the characteristics of low operating cost, robust maneuverability and high speed [4–5].

Automatic airborne video processing is one challenge in using airborne platform to collect traffic information. With the advances of computer vision technology, several airborne video processing softwares are developed to extract vehicle trajectory for traffic flow study [6–7], traffic flow monitoring [8–9] or traffic incident detection [5]. Because of the challenges in airborne video processing, researchers kept on improving the computer vision systems [7, 10]. One way is to focus the analysis on the road area, which can remove extraneous information out side of the road area leading to mismatch of feature points in image registration, or vehicle tracking [10]. Another merit is that it could focus computation effort on the roadway and improve the computation speed.

This study is inspired by DU and HICKMAN [10], in which road mask detection is used to improve vehicle detection and tracking. To improve the computer vision

system in previous research [5], a robust and fast road area detection algorithm is needed. In this work, the road to be tracked is a low volume road from cruising UAV which causes the failure of the algorithm proposed in Ref. [10], which is only suitable for the dense traffic road in video from geo-static UAV. Another challenge is that the road marks are partly covered by snow, which makes most of the current algorithms do not work well. So the research aim of the work is to propose a robust and fast road estimation method for note-well-marked roads in UAV video to improve the airborne video processing algorithm. This is one of the continue efforts to improve the software used in our previous work [5].

2 Literature review

A large number of road detection algorithms have been developed for various purposes. Videos from cameras on different platforms have different characteristics, which mainly include ground platform (e.g., vehicle) [11], low orbit platform (e.g., helicopter and UAV) and high orbit platform (e.g., satellite) [10]. The roads in the video from moving vehicle usually have vanishing points occupying most part of the imagery, while the roads in the video from low orbit platform are usually parallel lines with clear road edges. This work focus on road boundary detection algorithm for the video collected from UAV, only algorithms for this kind of video are investigated.

Most of the road boundary detection algorithms can be divided into two categories: feature-based and model-base methods. The feature-based methods locate the road areas using segmentation methods whereas the model-based methods represent the lane boundaries by mathematical models. Feature-based methods extract and analyze local lane features in order to separate the lane from background by pixel. Model-based methods normally incorporate various constraints during the detection stage to minimize the error and provide a simple description of the lane with mathematical models.

Features commonly used in lane detection are color, edge, texture, or hybrid of them. In Ref. [12], a color-based scheme was proposed to detect various lanes. Although the color is easily extracted, it is also easily affected by light changes. Thus, another trend to detect road boundary is based on edge features. JANG and HONG [13] incorporated the concept of the Hough transformation based approach into a line segment grouping to find favorable line segments. LIN et al [14] found different lane candidates from gradient space through morphological operators and Hough transform. This method does not work well when the road is not well painted. Texture is another useful feature for detecting lanes from unstructured road images. In Ref.

[15], road area is separated according to the difference of the texture between the road surface and surrounding environment. Usually, a hybrid scheme which integrates multiple features together will perform better than single one in road boundary detection.

Compared with the feature-based scheme, the model-based scheme performs more robustly since it can collect lots of lane samples with different patterns, occlusions, or shadows to construct a good lane detector. KLUGE and LAKSHMANAN [16] described a likelihood of image shape lane detection algorithm based on a deformable template approach. In a similar way, NIU [17] used a geometric active-contour model, which is a geometric alternative solution to the active- contour model to overcome its limitation. However, roads with sudden changes in asphalt color would cause problems as the road surface is treated as one single object.

Most of the existing methods mentioned above detect road boundary depending on the clues such as road color, texture or edges. In Refs. [10] and [18], the vehicle motion information is used as a clue for road detection, which works well on the busy road. Most of these methods work well for specific scenario, such as video with vanish point or with enough vehicle movement information. The video collected from cruising UAV varies in spatial-temporal space, which makes most of the methods not robust. Therefore, the algorithm based on the fusion information would be robust for this kind of video; while some characteristics do not work, and others could still support the algorithm making a proper decision.

3 Modeling basis

This section is started by introducing the basic idea to propose a method based on information fusion. Then, the basic concept of Dempster-Shafer theory of evidence is presented, which will be used in the next section.

3.1 Concept overview

Road detection algorithm is a decision making process based on various evidences. Generally, the more the clues are considered, the more robust the algorithm is. Because when some evidences are not available, other evidences can still support the decision making. Most of the current road detection methods are not based on the fusion information. On the contrary, the human vision could detect road robustly based on the multisource information fusion. For example, human could recognize the road area with part of the road marks covered by snow and can also distinguish between lanes and vehicle traces on the snow ground, depending on the fusion information of road color, texture, width and even the motion of the vehicles.

Dempster-Shafer theory of evidence is an information fusion method, which could deal with ignorance and missing information. A road boundary detection method based on this theory is proposed. Kalman filter method is used to keep tracking the road, which could give the detection result when the evidence is weak. The proposed algorithm should be computational efficient and perform robustly under great variance of the road color and when part of the road edge is covered by snow, which is suitable to process the video from the cruising UAV.

3.2 Dempster-Shafer theory of evidence

Dempster-Shafer theory (DST), first stated by Dempster in 1960s and later extended in 1970s by SHAFER [19], is capable of representing uncertainty as well as ignorance in statistical measurements. DST implies a type of uncertainty associated with conditions of ambiguity through the data by dealing with ignorance and missing information. The method can decrease the amount of information uncertainty by applying a combination rule to combine the confidence of different information sources, resulting in a more precise definition of hypothesis. DST is essentially a generalized Bayesian statistical theory [19].

Assume that f is a variable with a domain set Θ , f may also be treated as a question or proposition and Θ is a set of proposition or mutually exclusive and exhaustive hypothesis [20]. In DST, Θ is called the “frame of discernment” which is denoted as $\Theta = \{h_1, \dots, h_n\}$. The power set of all possible subsets of Θ , including itself and the empty set \emptyset , is 2^Θ , i.e., $2^\Theta = \{\emptyset, \{h_1\}, \dots, \{h_n\}, \{h_1 \cup h_n\}, \dots, \{h_{n-1}, h_n\}, \dots, \Theta\}$. Usually, some sources of information (SOI) are capable of providing distinguishable information for some subsets of Θ , which is denoted as S , i.e., $S \in 2^\Theta$. A mass function, also known as a basic belief or basic probability assignment, $m: 2^\Theta \rightarrow [0, 1]$ is a function satisfying

$$\begin{cases} m(\emptyset) = 0 \\ m(S) \geq 0, \forall S \in \Theta \\ \sum_{S \in \Theta} m(S) = 1 \end{cases} \quad (1)$$

where $m(S)$ is the belief provided by a source of information of S , which reflects how strongly the source of information supports S . There is no belief for \emptyset and all assigned mass values sum to unity. The subsets S of Θ with non-zero mass values are called focal elements. Equation (1) makes DST can handle both compound sets and singletons, while probabilistic approaches can only handle singleton focal elements.

Belief and plausibility are two other common

evidential measures that are derived from the mass function as

$$\begin{cases} B(\emptyset) = 0 \\ B(S) = \sum_{T \subset S, T \neq \emptyset} m(T) \end{cases} \quad (2)$$

$$\begin{cases} P(\emptyset) = 0 \\ P(S) = \sum_{S \cap T \neq \emptyset} m(T) \end{cases} \quad (3)$$

where S and T are subsets of Θ ; B and P are belief and plausibility of S and T , respectively; $B(S)$ and $P(S)$ represent the exact and possible supports to S , respectively. The interval $[B(S), P(S)]$ can be interpreted as the upper and lower bound of probability.

DST provides a way to combine the mass values assigned by different sources of information. Rule of combination fuses the mass functions m_i obtained from n sources of information, it can be calculated according to the following equations:

$$\begin{cases} m(\emptyset) = 0 \\ m(S) = \frac{\sum_{S_1 \cap \dots \cap S_n = S} \prod_{i=1}^n m_i(S_i)}{1 - K} \end{cases} \quad (4)$$

where K represents the degree of conflict given by

$$K = \sum_{S_1 \cap \dots \cap S_n = \emptyset} \prod_{i=1}^n m_i(S_i) \quad (5)$$

There are several ways of making the final decision using the DST framework. Road boundary detection is a classification problem to determine whether the candidate is road boundary or not. Hence, the final decision is made by selecting the hypothesis that produces the maximum aggregation of the mass values using the following equation as

$$X = \arg \max_{A \subset \Theta} (m(A)) \quad (6)$$

4 Evidences for road detection

Source of information (SOI) selection is the crucial part in application of Dempster-Shafer theory of evidence. This section starts by describing the selection of SOIs for road boundary detection evidences. Next, the details of the SOIs for DST are analyzed, which will be used in Section 5.

4.1 Source of information selection

There are a lot of clues for road boundary decision making, such as road surface color, edge and texture. As road texture takes more computation resources than road color, only road color is considered, which indicates road surface material as texture. The video is collected by a UAV hovering over a highway section or cruising along

the highway according to the planned flight route. So, the road direction or the road width will not change suddenly. Road direction and width are also considered road boundary clues. Thus, the road boundary is detected according to the follow clues:

1) The color is similar to the road color. On the same road section, the color of the road surface usually does not change dramatically.

2) The road direction is similar to long lines. The road boundaries are usually long parallel lines.

3) The road width is similar to the predefined one. According to the camera lens length and the UAV height, the road width in pixel coordinate system could be estimated roughly.

4) The road parameter is similar to the predicted ones using quick Kalman filter model. Road parameters in polar coordinates are tracked using Kalman filter model.

If a larger number of the above evidences support an edge candidate, this edge would more probably be a road boundary.

4.2 Color space

Red-green-blue (RGB) color space is used for several reasons. First, RGB color space ensures simplicity, effectiveness and speed, according to the recommendations of other researchers [19]. Second, RGB color space retains all color information and supplies more information than the gray color used in Ref. [6]. In the case of large changes in illumination, while the clue of color evidence is weak, other evidences such as road edge and road boundary tracking results could be used to support road boundary estimation. Furthermore, a dynamic road color updating scheme mentioned in next section is also adopted, which makes the proposed method keep tracking the correct road boundary when illumination changes suddenly.

The selection of SOI for road color requires analysis of the color distribution of the road area and non-road area. Normally, the road area color remains similar for the same road, while the non-road area usually varies along the road. According to the RGB color channel distribution analysis for studied data sets, road area color falls in a narrow range for red (R), green (G) and blue (B) channel and the variations of the value of B channel are smaller than the other two. Thus, the color value of B channel is considered an evidence of road surface. So, when most of the B channel color values from an area fall in this range, this area is very likely to be the road surface; or it is very likely not the road surface. The range is selected according to the statistic analysis within which most of the road surface color values fall in (e.g., 85%), which could be updated automatically after vehicle detection, which will be mentioned later.

4.3 Voting scheme for road edge detection

In the video from the camera on UAV cruising along the road, lane markings and road curbs separating roadside objects such as bushes and builds from the road area are important clues of road area. For highway, these lines are usually very long and are of the similar direction. The probable road edges are the long lines of the similar direction and have another side boundary line to which the distance is similar to the predefined road width. Road edge candidates are selected according to the road direction and robust line detection method modified from the method proposed in Ref. [13]. The algorithm is described as follows.

For the image I , the set of edge lines E is defined as a collection of straight lines named base line as

$$E = \{b_i = (\theta_i, \rho_i, l_i, d_i)\} \quad (7)$$

where b_i is the i th base line in the line set, $i=0, 1, \dots, N-1$ and N is the number of edge lines in the set. The tuple $(\theta_i, \rho_i, l_i, d_i)$ represents the line as road boundary candidate, where θ_i and ρ_i are the line parameters in polar coordinate system in image I , respectively, which defines a line as

$$x \cos \theta_i + y \sin \theta_i = \rho_i, \quad -\frac{\pi}{2} \leq \theta_i \leq \frac{\pi}{2} \quad (8)$$

where l_i is the length between two farthest endpoints of the base line b_i . The pixel density of the base line d_i is calculated by the following formula:

$$d_i = \frac{\sum_{j=0}^{k-1} p_j}{l_i} \quad (9)$$

where p_j is the project length of base line segment on x axis or y axis in the pixel coordinate in image I , and k is the number of the elementary line segment sets of base line b_i denoted as EB_i .

The algorithm to find base lines is as follows. Denote the i th elementary line segment (ELS) as e_i and the two polar parameters of e_i as $\theta(e_i)$ and $\rho(e_i)$, which represent the angle and the distance of e_i to the original point, respectively. Each e_i in EB_i satisfies the following condition as

$$|\theta_b - \theta(e_i)| \leq \Delta\theta_b + \frac{\Delta\theta_d}{\sqrt{l(e_i)}} \quad (10)$$

where θ_b is the angle of b_i , $\Delta\theta_b$ and $\Delta\theta_d$ are user-specified parameters and $l(e_i)$ denotes the length of e_i .

An extremely simple and fast method is proposed to replace the ‘‘lateral distance’’ calculation in Ref. [13], which needs more computation resources. The algorithm is as follows:

Step 1: Create a vector V_{base}^i and initialize all the

elements to 0 and the length of vector N is defines as

$$N_{base}^i = \begin{cases} h & \text{if } |\theta_i| \leq \frac{\pi}{4} \\ w & \text{if } |\theta_i| > \frac{\pi}{4} \end{cases} \quad (11)$$

where h and w are the height and width of image I , respectively.

Step 2: Assign the vector values according to the following method,

$$V_{base}^i [i_{start}, i_{end}] = 1 \quad (12)$$

where i_{start} and i_{end} are the start and end indexes of vector NV_{base}^i , respectively.

If $N_{base}^i = w$, i_{start} and i_{end} are assigned by the smaller and the bigger x coordinate value of e_i ; else, i_{start} and i_{end} are assigned by the smaller and the bigger y coordinate value of e_i .

Step 3: i_{min} and i_{max} are the first index and the last index of the non-zero vector element, respectively, s_i is the summary of V_{base}^i , the pixel density rate is calculated as

$$d_i = \frac{s_i}{i_{max} - i_{min}} \quad (13)$$

The highways studied in this work have the following characteristics: locally flat, defined by parallel road curbs or markings lengthwise and without sharp bends or roundabouts, and the road orientation can be determined using the method proposed in Ref. [21]. Let Θ define a set of base lines as follows:

$$\Theta = \{\theta_k = \angle e_k : \theta_k \in [0, \dots, \pi] | k = 0, \dots, N-1\} \quad (14)$$

where $\theta_k = \angle e_k$ denotes the orientation of the k th base line; L_{θ_k} is the sum of the length of all base lines having the same direction θ_k , and it is given by

$$L_{\theta_k} = \sum |e_i|, \text{ for all } \angle e_i = \theta_k \quad (15)$$

$$|e_i| = l_i \times d_i \quad (16)$$

Θ is divided into two sets (Θ_{major} and Θ_{minor}) according to L_{θ_k} using the K -means clustering method described in Ref. [21], with $K=2$. The road boundary candidates are as follows:

$$E_{candidate} = \{e_k \in E : \theta_k \in \Theta_{major}\} \quad (17)$$

where e_k is the k th longest of base line in Θ_{major} , $k=0, \dots, N_{candidate}-1$ and $N_{candidate}$ is the number of edge candidates. The length between two parallel base lines is

$$d = |\rho_i - \rho_j| \quad (18)$$

where ρ_i and ρ_j are the parameters of base line b_i defined in Eq. (7).

4.4 Road estimation using quick Kalman filtering

Because of the movement of the UAV along the road, the edge model parameters of the road boundary vary according to time. The road edge parameters constitute the state vector as

$$x_t = (a_t, b_t)^T \quad (19)$$

where a_t and b_t are the line parameters in Cartesian coordinates system transformed from polar coordinate system, and a_t and b_t are line slope and intercept, respectively. Kalman filter is a fast method which could estimate the internal state of a linear dynamic system from a series of noisy measurements. Road edge parameter is tracked using Kalman filter.

The state vector at time $t+dt$ is predicted by the following equation using the state of vector at time t . The state updating and observation equations of the dynamic system are as follows:

$$\begin{cases} x_t = x_{t-1} + W_{(0, \varrho)} \\ z_t = Hx_{t-1} + v_{0, R} \end{cases} \quad (20)$$

where x_t and x_{t-1} are the edge parameters at time t and $t-1$, respectively; H is the observation matrices; z_t is the system observation; $W_{(0, \varrho)}$ is the system noise and $v_{(0, R)}$ is the observation noise which both have zero mean, and variance matrices Q and R are set to diagonal matrices with constant elements; z_t is the y coordinate to the point on road edge. According to line formula in Cartesian coordinates system, H can be expressed as

$$H = \begin{bmatrix} Z_1 & 1 \\ \vdots & \vdots \\ Z_N & 1 \end{bmatrix} \quad (21)$$

where Z_1, \dots, Z_N are x coordinate values of points on the road edge.

5 Dempster-Shafer based road boundary detection

As illustrated in Fig. 1, the two crucial steps of DSRD are determination of mass values provided by SOIs and combination of the mass values to make the final decision. In this section, the methods to calculate mass values and make the final decision by combining the mass values using DST will be described in details.

5.1 Determination of mass values

In the use of evidence theory, the determination of mass functions is a delicate but key point, which is still an open issue in evidence theory [22–23]. The mass function is usually assumed to be given, e.g. by experts

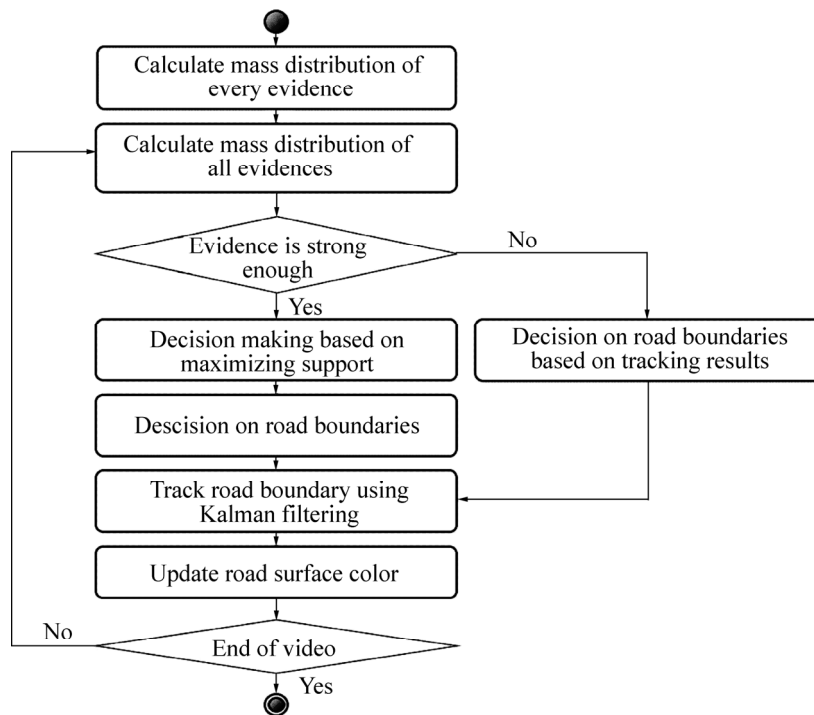


Fig. 1 Flowchart of road boundary detection using DST

[24], or derived from data [23, 25]. Most of the current mass function determination methods need sample data which have been clustered already. This kind of methods cannot be used in this study because of the sharp variation of the background outside the road area caused by the movement of the camera on cruising UAV. The method based on the “distance” of a point from a prototypical member is adopted to assign mass function, which is used for determining membership function in fuzzy theory [26].

The mass functions are listed in Table 1. The frame of discernment for road boundary detection problem is $A = \{C_1, C_2, C_1 \cup C_2\}$. C_1 is the road edge, C_2 is the non-road and $C_1 \cup C_2$ represents the vagueness of both road and non-road. The set of SOIs is $B = \{B_1, B_2, B_3, B_4, B_5\}$. B_1 is road color, B_2 is road direction, B_3 is road width, B_4 and B_5 are the variations of road parameters in polar coordinate system, which are direction and distance from origin point, respectively. $m\{B_1\}$, $m\{B_2\}$, $m\{B_3\}$, $m\{B_4\}$ and $m\{B_5\}$ and denoted as Δd and $\Delta \rho$ are the mass values

of B_1, B_2, B_3, B_4 and B_5 , respectively.

As analyzed in the above section, the road color value of B channel is within a narrow range noted as $[b_{low}, b_{up}]$. If most of the color values in an area fall in this range, this area is probably road surface. According to the tests, the range containing 85% of color values in road area is selected, as the range is too large when 100% of color value is considered. Denote the percentage of color values within $[b_{low}, b_{up}]$ as r_{color} , the mass function of color for C_1 is calculated by

$$p_{color} = r_{color} \times 0.85 \tag{22}$$

where 0.85 is an adjusting coefficient, which is set using experimental method. The road surface color value is within a narrow range and is usually different from non-road color. Hence, null probability mass is assigned to compound hypotheses of C_1 and C_2 . Since all the masses should sum to 1, the probability mass for non-road C_2 is $1 - p_{color}$.

The probability masses for road width are determined in a similar way. As UAV cruises along the planned flight rout, the width of the highway could be estimated according to camera lens length and UAV height roughly, which is noted as w_{design} . If the measured width of a pair of lines $w_{measure}$ is similar to w_{design} , this pair of lines would probably be the two sides of a road. The measure error of the road width is noted as $E_{measure}$ and threshold of the maximum measure error is noted as T_{width} . Then the mass function of road width for C_1 is

Table 1 Calculation of probability masses, support and plausibility

A	$m\{B_1\}$, color	$m\{B_2\}$, direction	$m\{B_3\}$, road width	$m\{B_4\}$, Δd	$m\{B_5\}$, $\Delta \rho$
C_1 road edge	p_{color}	$p_{direction}$	p_{width}	$p_{\Delta d}$	$p_{\Delta \rho}$
C_2 non-road	$1 - p_{color}$	$(1 - p_{direction})/2$	$(1 - p_{width})/2$	$1 - p_{\Delta d}$	$1 - p_{\Delta \rho}$
$C_1 \cup C_2$	0	$(1 - p_{direction})/2$	$(1 - p_{width})/2$	0	0

calculated by

$$p_{width} = \begin{cases} 1 & \text{if } |w_{design} - w_{measure}| \leq E_{error} \\ \frac{T_{width} - |w_{design} - w_{measure}|}{T_{width} - E_{error}} & \text{if } E_{error} < |w_{design} - w_{measure}| \leq T_{width} \\ 0 & \text{else} \end{cases} \quad (23)$$

Other objects such as vehicle tracks on the snow ground or the edges of buildings along the road may have similar direction of the road. So, the left probability masses are assigned to C_2 and $C_1 \cup C_2$ equally, which is $(1-p_{width})/2$.

For road direction, let D_{line} denote the detected line direction, D_{road} denote the road angle calculated in section 4.2, $E_{direction}$ be the measure error of the road angle and $T_{direction}$ be the threshold of the maximum measure error, the mass function of C_1 for road direction is calculated by

$$p_{direction} = \begin{cases} 1 & \text{if } |D_{road} - D_{line}| \leq E_{direction} \\ \frac{T_{direction} - |D_{road} - D_{line}|}{T_{direction} - E_{direction}} & \text{if } E_{direction} < |D_{road} - D_{line}| \leq T_{direction} \\ 0 & \text{else} \end{cases} \quad (24)$$

The other probability masses are assigned equally to C_1 and $C_1 \cup C_2$, which is $(1-p_{direction})/2$.

The UAV used in this study could record the UAV yaw speed and UAV flying speed with high temporal and spatial resolution for flying controlling purpose. Because the video is from the UAV cruising along the road, the movement of the road can be reflected by the movement of the camera platform. Denote the UAV yaw speed and flying speed as v_{yaw} and v_{fly} , the variation of yaw angle speed as Δ_{yaw} , the measure error of yaw angle speed as ΔE_{yaw} and the threshold of the maximum measure error as ΔT_{yaw} , then the mass function of C_1 for road direction variation is

$$p_{\Delta direction} = \begin{cases} 1 & \text{if } |\Delta d_{ir}| \leq E_{\Delta yaw} \\ \frac{T_{\Delta yaw} - |\Delta d_{ir}|}{T_{\Delta yaw} - E_{\Delta yaw}} & \text{if } E_{\Delta yaw} < |\Delta d_{ir}| \leq T_{\Delta yaw} \\ 0 & \text{else} \end{cases} \quad (25)$$

where ρ_t is the distance from the origin of coordinates of the line in polar coordinate system. The variation of ρ_t could be calculated according to Δd and v_{fly} . Denote the measure error of ρ_t as ΔE_ρ and the threshold of the maximum measure error as ΔT_ρ , then they can be calculated according to the follow formula as

$$\begin{cases} E_{\Delta \rho} = \sin(E_{\Delta yaw}) \times v_t \times \Delta t \\ T_{\Delta \rho} = \sin(T_{\Delta yaw}) \times v_t \times \Delta t \end{cases} \quad (26)$$

The mass function of C_1 for ρ can be calculated according to the follow formula as

$$p_{\Delta \rho} = \begin{cases} 1 & \text{if } |\Delta \rho| \leq E_{\Delta \rho} \\ \frac{T_{\Delta \rho} - |\Delta \rho|}{T_{\Delta \rho} - E_{\Delta \rho}} & \text{if } E_{\Delta \rho} < |\Delta \rho| \leq T_{\Delta \rho} \\ 0 & \text{else} \end{cases} \quad (27)$$

If Δd_{ir} and $\Delta \rho$ of the road edge candidate are similar to the values from UAV flight record, it would be probably road boundary, or it is not. As all the masses should sum to 1, the probability masses for C_2 of B_4 and B_5 are $1-p_{\Delta direction}$ and $1-p_{\Delta \rho}$, respectively.

5.2 Combining outcomes of SOIs using DST

To obtain a reliable decision, five different SOIs are used, as listed in Table 1. As stated in Section 3, the mass values of the individual SOIs can be calculated according to Eq. (4). In order to illustrate Dempster’s rule of combination which fuses the mass functions obtained from multiple source of information, an easy example of two sources of information of a road edge candidate is given in Table 2. Five sources of information can be calculated in a similar way by a recursion process. According to Eq. (4), the combinations of the mass values for different hypotheses are

$$k = 0.06 + 0.32 = 0.38 \quad (28)$$

$$m(\{\text{road boundary}\}) = \frac{0.48 + 0.06}{1 - 0.38} = 0.8710 \quad (29)$$

$$m(\{\text{non-road}\}) = \frac{0.04 + 0.04}{1 - 0.38} = 0.1290 \quad (30)$$

$$m(\{\text{road boundary} \cup \text{non-road}\}) = \frac{0}{1 - 0.38} = 0 \quad (31)$$

6 Performance evaluations

In order to evaluate the performance of the proposed algorithm, two field experiments were

Table 2 An example of mass values of a road boundary candidate

A	$m_1\{B\}$ color	$m_2\{B\}$, direction
C_1 road edge	0.6	0.8
C_2 non-road	0.4	0.1
$C_1 \cup C_2$	0	0.1

conducted, one was on a low volume expressway and another was on a highway in urban area. The road

boundary detection performance and the effects for improving vehicle detection and tracking will be analyzed in this section.

6.1 Experiment description

The algorithm proposed was implemented with python using Numpy1.7 and integrated into the software TIEP1.0 (Traffic Information Extraction Platform for UAV Data1.0), which was developed based on our previous study [5]. The UAV used in this experiment is a four-rotor helicopter (MD4-1000), which can collect video data and flight records.

The first experiment was conducted on a four-lane low volume expressway in the desert area in Shinkiang, China. The video data were collected in February, 2012 after a heavy snow using a cruising UAV which traveled about 8 km. In the video, there were vehicle tracks on the background as noise and parts of the road marks were covered by snow. There were 500 frames selected for testing purpose. The second experiment was carried out on an eight-lane highway in suburban area in Shanghai, China, in July, 2013. The traffic flow rate was higher,

which was about 2400 vehicles per hour. There were 1000 frames selected for testing purpose.

6.2 Experiment results

The proposed algorithm has been tested on a laptop computer with two 2.6 GHz processors (Intel i5-3320M). If both sides of the road edges are detected correctly compared with manual detection results, then road boundary is considered to be detected correctly. Because the purpose of road detection is to improve the vehicle detection and tracking, the road detection does not need pixel level of accuracy. If the road boundary covers almost all parts of the road area and is accurate enough for vehicle detection and tracking, the result can be considered to be correct (Fig. 2). The detection quality is measured using the well-known notations: T_P is the road detected correctly, F_N is the non-road object detected as road, and F_P is road not correctly detected as road. Then, the detection rate (DR, R_D), true positive rate (TPR, R_{TP}) and false positive rate (FPR, R_{FP}) are calculated according to the following equations:

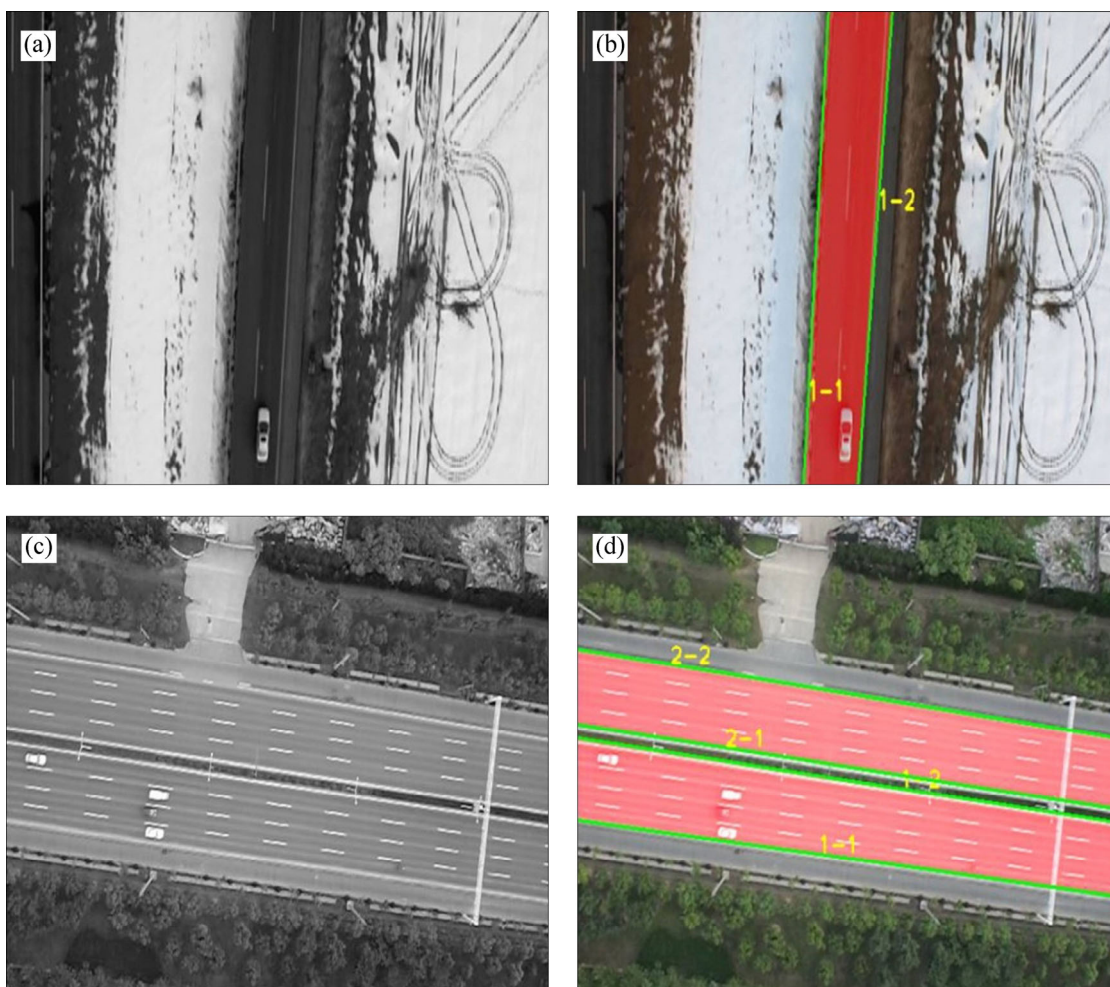


Fig. 2 Experimental results: (a) Input image of Experiment 1; (b) Road boundary detection result of Experiment 1; (c) Input image of Experiment 2; (d) Road boundary detection result of Experiment 2

$$R_{TP} = \frac{T_p}{T_p + F_p} \tag{32}$$

$$R_{FP} = \frac{F_p}{T_p + F_p} \tag{33}$$

$$R_D = \frac{N_{correct}}{N_{road} + N_{pseudo}} \tag{34}$$

where N_{road} is the number of frames containing roads, N_{pseudo} is the number of frames in which non-road objects are detected as roads and $N_{correct}$ is the number of the frames in which roads are detected correctly.

The proposed methods are tested with two field data sets mentioned above. In order to compare the effects of the factors for road boundary detection, several methods modified from the proposed algorithm are tested, in which some of the evidences are not considered. As shown in Table 3, the proposed algorithm has high detection accuracy on both data sets, which is above 98%, and the color and width are evidences which can improve the detection quality significantly. When road tracking information is not considered, the FPR increases

Table 3 Detection analysis of on two data sets

Method	Data set 1			Data set 2		
	$R_D/\%$	$R_{TP}/\%$	$R_{FP}/\%$	$R_D/\%$	$R_{TP}/\%$	$R_{FP}/\%$
Proposed method	100.00	100.00	0.00	98.00	99.80	0.20
No tracking	96.40	97.57	2.43	96.20	97.96	2.04
No color	96.60	99.38	0.62	96.30	99.79	0.21
No road width	97.20	99.18	0.82	94.60	99.58	0.42

significantly which is caused by the missed detection of the road.

The average computation time of the proposed algorithm is about 0.08 s. For the video processing method, the frame is retrieved every 6 frames from video file. The camera sampling rate is 30 Hz. So, the least time for video time processing is 0.2 s. Thus, the proposed algorithm is fast enough for real time processing. Furthermore, the computation speed could be improved by rewriting the algorithm using C++.

6.3 Application of road boundary detection for vehicle detection and tracking

The road boundary detection has many benefits for vehicle detection and tracking. Firstly, the image registration accuracy could be improved using the control points within or near the road boundary. Second, the road boundary can be applied to removing false detections and to reducing the computation time. Furthermore, road surface color can be updated dynamically during road detection process, which is needed for image segmentation to detect static vehicles for cruising UAV. The application of road boundary detection in vehicle detection and tracking is shown in Fig. 3.

According to the tests on the two data sets mentioned in the above section, the vehicle detection and tracking have been improved significantly. By using road boundary information, the vehicle detection and tracking rate are improved from 90% to 92.7% for data set 1 and all static vehicles could be detected successfully. For data set 2, the detection rate is improved from 82% to 87.5%. Also, the computation time has decreased by 5% and 8.3% for data sets 1 and 2, respectively.

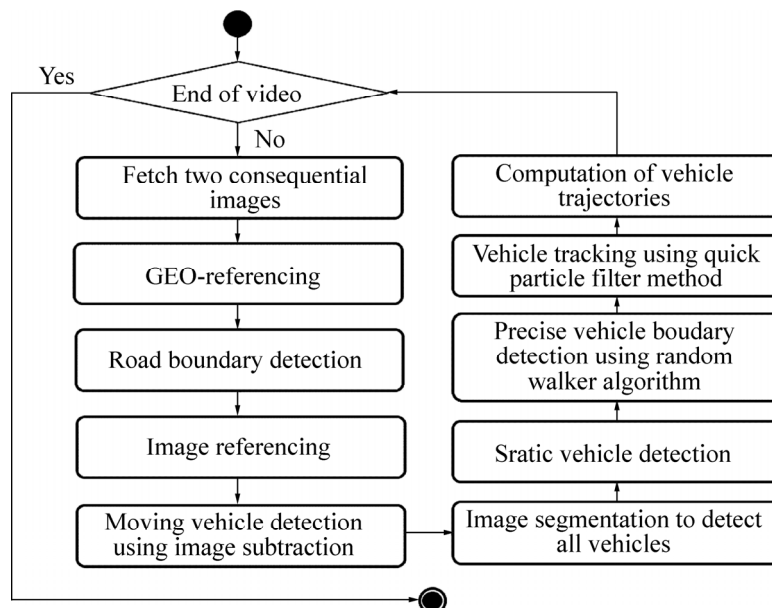


Fig. 3 Flow chart of vehicle detection and tracking

7 Conclusions

1) A robust road boundary detection method named DSRD is proposed, with ultimate goal to improve vehicle detection and tracking in UAV video. DSRD uses Dempster-Shafter theory of evidence to detect the road boundary using fusion information of road edges, surface color, width and road tracking information.

2) In order to test the performance of the proposed algorithm, DSRD was tested with two field data sets. The experiments show that DSRD has high accuracy and works robustly.

3) DSRD is integrated as one component of a computer vision system for UAV video processing. The test results show that the proposed approach could improve vehicle detection and tracking accuracy significantly, while the computation speed is increased.

4) UAV is considered a promising traffic information collection platform due to its ability to get detailed microscopic traffic information, low operation cost and convenient deployment. However, processing airborne video is still challenging. The rapid development of computer vision will supply more robust and accurate algorithms for vehicle detection and tracking. Other methods to improve the accuracy of vehicle trajectories such as filter technology will be studied in the near future. Also, the vehicle trajectory data collected from UAV will be used for driving behavior study.

References

- [1] HICKMAN M, MIRCHANDANI P. Airborne traffic flow data and traffic management [C]// BEAL J G. 75 years of the fundamental diagram for traffic flow theory: Greenshields symposium. Washington D C: Transportation Research Board, 2011: 121–133.
- [2] DAAMEN W, LOOT M, HOOGENDOORN S P. Empirical analysis of merging behavior at freeway on-ramp [J]. Transportation Research Record: Journal of the Transportation Research Board, 2010, 2188: 108–118.
- [3] OSSEN S, HOOGENDOORN S P. Heterogeneity in car-following behavior: Theory and empirics [J]. Transportation Research Part C-Emerging Technologies, 2011, 19(2): 182–195.
- [4] LIU Xiao-feng, PENG Zhong-ren, CHANG Yun-tao, ZHANG Li-ye. Multi-objective evolutionary approach for UAV cruise route planning to collect traffic information [J]. Journal of Central South University, 2012, 19(12): 3614–3621.
- [5] ZHANG L, PENG Z, SUN D J, LIU Xiao-feng. A UAV-based automatic traffic incident detection system for low volume roads [C]// 92rd Annual Meeting of the Transportation Research Board. Washington D C, 2013.
- [6] HOOGENDOORN S P, van ZUYLEN H J, SCHREUDER M, GORTE B, VOSSelman G. Microscopic traffic data collection by remote sensing [J]. Transportation Research Record: Journal of the Transportation Research Board, 2003, 1855: 117–125.
- [7] KNOOP V L, HOOGENDOORN S P, van ZUYLEN H J. Processing traffic data collected by remote sensing [J]. Transportation Research Record: Journal of the Transportation Research Board, 2009, 2129: 55–61.
- [8] COIFMAN B, MCCORD M, MISHALANI R, ISWAKT M, JI Y. Roadway traffic monitoring from an unmanned aerial vehicle [J]. IEEE Journal on Intelligent Transport Systems, 2006, 153(1): 11–20.
- [9] ANGEL A, HICKMAN M, MIRCHANDANI P, CHANDNANI D. Methods of analyzing traffic imagery collected from aerial platforms [J]. IEEE Transactions on Intelligent Transportation Systems, 2003, 4(2): 99–107.
- [10] DU X, HICKMAN M. Estimating a road mask to improve vehicle detection and tracking in airborne imagery [J]. Transportation Research Record: Journal of the Transportation Research Board, 2012, 2291: 93–101.
- [11] WANG Y, SHEN D, TEOH E K. Lane detection using spline model [J]. Pattern Recognition Letters, 2000, 21(8): 677–689.
- [12] WANG Y, SHEN D, TEOH E K. Lane detection using catmull-rom spline [C]// IEEE International Conference on Intelligent Vehicles. Stuttgart, 1998: 51–57.
- [13] JANG J H, HONG K S. Fast line segment grouping method for finding globally more favorable line segments [J]. Pattern Recognition, 2002, 35(10): 2235–2247.
- [14] LIN H, KO S, SHI W, KIM Y, KIM H. Lane departure identification on highway with searching the region of interest on hough space [C]// International Conference on Control, Automation and Systems 2007. Seoul, 2007: 1088–1091.
- [15] GRAOVAC S, GOMA A. Detection of road image borders based on texture classification regular paper [J]. International Journal of Advanced Robotic Systems, 2012, 9(242): 1–12.
- [16] KLUGE K, LAKSHMANAN S. Lane boundary detection using deformable templates: Effects of image subsampling on detected lane edge [J]. Recent Developments in Computer Vision Lecture Notes in Computer Science, 1996, 1035: 329–339.
- [17] NIU X T. A semi-automatic framework for highway extraction and vehicle detection based on a geometric deformable model [J]. ISPRS Journal of Photogrammetry and Remote Sensing, 2006, 61(3): 170–186.
- [18] PLESS R. Detecting roads in stabilized video with the spatio-temporal structure tensor [J]. Geoinformatica, 2006, 10(1): 37–53.
- [19] SHAFER G. A mathematical theory of evidence [M]. Princeton, New Jersey: P U Press, 1976: 35–41.
- [20] GHASEMI J, GHADERI R, MOLLAEI M, MOLLAEI M, HOJJATOLESLAMI S A. A novel fuzzy Dempster-Shafer inference system for brain MRI segmentation [J]. Information Sciences, 2013, 223: 205–220.
- [21] LAI A H S, YUNG N H C. Lane detection by orientation and length discrimination [J]. Systems, IEEE Transactions on Man, and Cybernetics, Part B: Cybernetics, 2000, 30(4): 539–548.
- [22] XU P D, DENG Y, SU X Y, MAHADEVAN S. A new method to determine basic probability assignment from training data [J]. Knowledge-based Systems, 2013, 46: 69–80.
- [23] BEN CHAABANE S, SAYADI M, FNAIECH F, BRASSART E, BETIN F. A new method for the estimation of mass functions in the Dempster-Shafer's evidence theory: Application to colour image segmentation [J]. Circuits Systems and Signal Processing, 2011, 30(1): 55–71.
- [24] LU Y H, TRINDER J C, KUBIK K. Automatic building detection using the Dempster-Shafer algorithm [J]. Photogrammetric Engineering and Remote Sensing, 2006, 72(4): 395–403.
- [25] WANG H, LIU J, AUGUSTO J C. Mass function derivation and combination in multivariate data spaces [J]. Information Sciences, 2010, 180(6): 813–819.
- [26] ZIMMERMANN H J, ZYSNO P. Quantifying vagueness in decision-models [J]. European Journal of Operational Research, 1985, 22(2): 148–158.